ELSEVIER

Journal of Molecular Structure 598 (2001) 171–195

Journal of
MOLECULAR
STRUCTURE

www.elsevier.com/locate/molstruc

1,2-Diiododisilane and 1,1,2,2-tetraiododisilane: a reinvestigation of the molecular structures and vibrational properties by gas-phase electron diffraction, temperature dependent Raman spectroscopy, and ab initio molecular orbital- and density functional calculations

Tore H. Johansen[a,*], Karl Hassler[b], Günter Tekautz[b], Kolbjørn Hagen[a]

[a]*Department of Chemistry, Norwegian University of Science and Technology, NTNU, N-7491 Trondheim, Norway*
[b]*Institut für Anorganische Chemie, Technische Universität, Stremayrgasse 16, A-8010 Graz, Austria*

Received 21 February 2001; revised 9 April 2001; accepted 9 April 2001

Abstract

The molecular structure, internal rotation and vibrational properties of 1,2-diiododisilane (DIDS), $IH_2Si–SiH_2I$, and 1,1,2,2-tetraiododisilane (TIDS), $I_2HSi–SiHI_2$, have been reinvestigated using gas phase electron diffraction (GED) data at temperatures of 55 (DIDS) and 155 (TIDS) °C, together with Raman spectroscopy, and ab initio molecular orbital (MO)- and density functional (DFT) calculations. The title compounds exist in the gas and liquid phases as a mixture of two conformers, *anti* (C_{2h}), with a torsion angle ϕ (XSiSiX) = 180°, and *gauche* (C_2), with a torsion angle ϕ (XSiSiX) $\approx$ 60° (X = I (DIDS), X = H (TIDS)). Some structural parameter values obtained from the GED dynamic model refinements, using results from the theoretical calculations as constraints, were as follows (*anti* values with estimated 2σ uncertainties): For DIDS: Bond lengths (r_g): r(Si–Si) = 2.315(26) Å, r(Si–I) = 2.447(6) Å. Bond angles ($\angle_\alpha$): ∠SiSiI = 107.5(10)°, ∠ISiH = 109.8(5)°. For TIDS: Bond lengths (r_g): r(Si–Si) = 2.364(30) Å, r(Si–I) = 2.450(6) Å, Bond angles ($\angle_\alpha$): ∠SiSiI = 107.2(4)°, ∠ISiH = 109.9(2)°, ∠ISiI = 111.7(3)°. Raman vibrational spectra for various temperatures are presented and analysed aided by normal coordinate calculations and the ab initio MO- and DFT results. From intensity variations with temperature of four band pairs for DIDS and two pairs for TIDS, conformational energies in the liquids were determined from van't Hoff plots. $\Delta H^0 (\approx \Delta E^0)$ values of 0.31 ± 0.14 kcal mol^{-1} and 0.14 ± 0.10 kcal mol^{-1} were obtained for DIDS and TIDS respectively, *gauche* being the low energy conformer for both disilanes.

Keywords: Iododisilanes; Torsional potential functions; Gas electron diffraction; Vibrational spectroscopy

1. Introduction

The structural and conformational properties of halogen-substituted disilane molecules have been our interest for some time. We have recently reported experimental molecular structures and torsional potential functions for 1,1,2-triiododisilane ($I_2HSi–SiH_2I$) [1] and 1,1,2,2-tetrachlorodisilane ($Cl_2HSi–SiHCl_2$) [2] using gas-phase electron diffraction (GED) data, aided by results from infrared (IR) and Raman vibrational spectroscopic studies [1–3]. For 1,1,2-triiododisilane a rather flat torsional potential was found [1], indicating a large degree of unhindered internal rotation. In the investigation on 1,1,2,2-tetrachlorodisilane constraints

* Corresponding author. Tel.: +47-73-5907-52; fax: +47-73-5962-55.
E-mail address: torej@pop.chembio.ntnu.no (T.H. Johansen).

0022-2860/01/$ - see front matter
PII: S0022-2860(01)00631-7

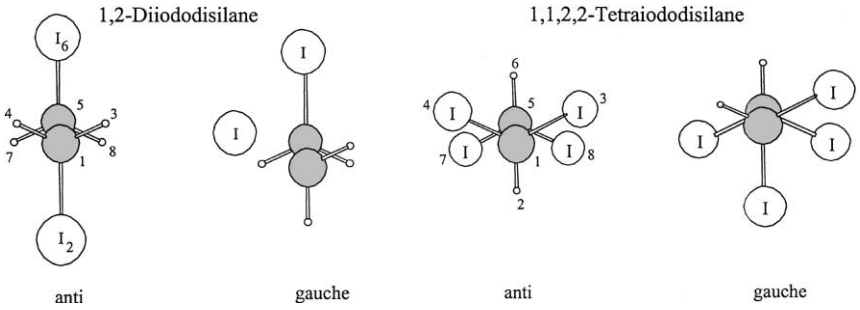

Fig. 1. Molecular models of the possible *anti* and *gauche* conformers of 1,2-diiododisilane (DIDS) and 1,1,2,2-tetraiododisilane (TIDS).

from Raman energy results [3] had to be used in the potential parameter refinements [2].

In 1991, Røhmen et al. published GED results for 1,2-diiododisilane (DIDS) and 1,1,2,2-tetraiododisilane (TIDS), based on purely static models, and with shrinkage corrections calculated from general valence force fields [4]. At about the same time, Hassler and Põschl published extensive IR and Raman spectroscopic data, including the d_4 and d_2 isotopomers, for DIDS and TIDS, respectively [5]. In a comparison of the parameter values found for the Si–Si bond distance in the title compounds by Røhmen et al. with the range of values discussed in the paper on 1,1,2-triiododisilane [1], we concluded that the *r*(Si–Si) parameter was found unusually large in the investigations by Røhmen et al. [4]; with values of 2.380–2.389 Å (r_g), compared to the value of only 2.329(12) Å (r_g) in the 1,1,2-triiododisilane. Based on the more elaborate models deemed necessary for the 1,1,2-triiodo- and 1,1,2,2-tetrachlorodisilanes [1,2], where geometry constraints and modified quantum mechanical force fields were used in the analyses, as well as explicit modeling of the Si–Si torsional motion using Fourier cosine potentials, revisiting the DIDS and TIDS molecules seemed like an inevitable undertaking.

In the present reinvestigation more elaborate dynamic theoretical models similar to the ones previously used in the studies of 1,1,2-triiododisilane [1] and 1,1,2,2-tetrachlorodisilane [2] have been employed. It was hoped that these improved models would remove some of the discrepancies between the earlier reported, and surprisingly larger, Si–Si bond distances [4] and the values obtained for this bond in recent works [1,2], which were more consistent with established experimental data [6–15]. In the present investigation, we have indeed obtained experimental results that support the view that the Si–Si bond distance in the two title compounds with high certainties should be lower than earlier reported [4]. Our new results falls more into the range of normal values observed for this type of bond, judging from both experimental and theoretical data data found in the literature [6–15].

Consequently, the experimental and theoretical findings in a reinvestigation of the 1991 GED data for the molecules 1,2-diiododisilane (DIDS) and 1,1,2,2-tetraiododisilane (TIDS) will be described in this paper (Fig. 1), aided by recently recorded IR- and variable temperature Raman spectroscopic data, and ab initio molecular orbital (MO) and density functional theory (DFT) calculations, including the use of effective core potentials [16–18] in representing the core electrons of the iodine atoms (HW-ECP; SBK-ECP; cf. Ref. [1]).

2. Experimental section

2.1. Synthesis of the compounds

Samples of DIDS and TIDS were prepared according to the literature [5] by protodearylation of PhH_2SiSiH_2Ph and $Ph_2HSiSiHPh_2$ with hydrogen iodide (HI). The iododisilanes were purified by fractional distillation under vacuum, and the purity was checked by ^{1}H- and ^{29}Si-NMR spectroscopy.

2.2. Vibrational spectroscopy

Raman spectra in the range 3000–40 cm^{-1} were

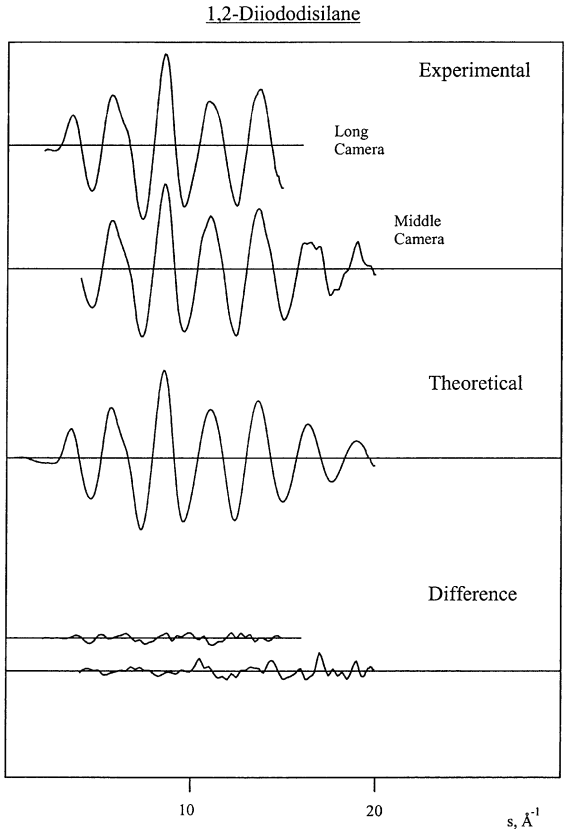

Fig. 2. Intensity curves ($sI_m(s)$) for 1,2-diiododisilane. The experimental curves are the average molecular intensity data obtained from the plates of the two camera distances (Long Camera and Middle Camera). The theoretical curve was calculated from the structural parameters given in Table 1 (dynamic model). The difference curves result from subtracting the relevant part of the theoretical curve from each of the experimental curves.

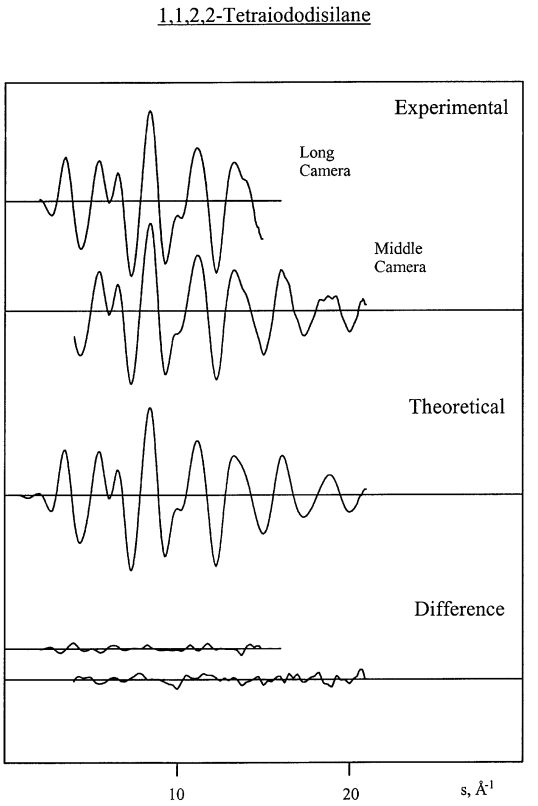

Fig. 3. Intensity curves ($sI_m(s)$) for 1,1,2,2-tetraiododisilane. The experimental curves are the average molecular intensity data obtained from the plates of the two camera distances (Long Camera and Middle Camera). The theoretical curve was calculated from the structural parameters given in Table 1 (dynamic model). The difference curves result from subtracting the relevant part of the theoretical curve from each of the experimental curves.

recorded with a T 64000 spectrometer of Jobin-Yvon equipped with a triple monochromator. The spectra were excited with the green (514 nm) line of an Argon-laser. All samples were distilled or condensed into 1 mm capillaries which then were sealed under a nitrogen atmosphere. Low temperature Raman spectra were obtained with the help of a cryostat equipped with quartz windows and a copper block which could be cooled with liquid nitrogen and heated resistively. The capillary was mounted on the copper block whose temperature was monitored with a thermocouple. To avoid any deposition of ice, the cryostat was evacuated during the measurements.

2.3. Gas electron diffraction

Electron-diffraction patterns were recorded with the Balzers Eldigraph KD-G2 (42 kV) at the University of Oslo [19] on Kodak Electron Image plates with an average nozzle-tip temperature of 328 K (DIDS) and 428 K (TIDS). The average electron wavelength was $\lambda = 0.0590$ Å. Five diffraction photographs from the long camera (LC) and six diffraction photographs from the middel camera (MC) camera distances were used in the analysis for DIDS, the corresponding numbers for TIDS were 5 (LC) and 5 (MC). Further details about experimental conditions are found in Ref. [4]. A calculated background [20] was subtracted from the data for each plate to yield experimental

Table 1
Experimental structural and potential parameters for 1,2-diiododisilane and 1,1,2,2-tetraiododisilane, from both dynamic and static models of the *anti* and *gauche* conformers (Distances (r_g) are in ångstrøms (Å), angles ($\angle_\alpha$) in degrees. Parenthesized values are 2σ, where σ include estimates of uncertainty in voltage/nozzle heights and of correlation in the experimental data. Values in brackets are taken from or estimated from the DFT calculations). The static model refinements were performed with shrinkage corrections calculated from ab initio force fields with all vibrational modes included, except that perpendicular amplitude correction values were held as used in the dynamic case

Gas electron diffraction

	Dynamic				Static			
	1,2-Diiododisilane		1,1,2,2-Tetraiododisilane		1,2-Diiododisilane		1,1,2,2-Tetraiododisilane	
r_g, $\angle_\alpha$	*Anti* (C_{2h})	*Gauche* (C_2)	*Anti* (C_{2h})	*Gauche* (C_2)	*Anti*	*Gauche*	*Anti*	*Gauche*
r(Si–Si)	2.315(26)	2.325(26)	2.364(30)	2.363(30)	2.319(24)	2.327(24)	2.346(24)	2.343(24)
r(Si–I)	2.447(6)	2.434(6)	2.450(6)	2.433(6)	2.449(6)	2.434(6)	2.450(4)	2.438(4)
r(Si–I)	2.447(6)	2.434(6)	2.450(6)	2.449(6)	2.449(6)	2.434(6)	2.450(4)	2.448(4)
r(Si–H)	[1.528]	[1.533]	[1.531]	[1.529]	[1.528]	[1.532]	[1.531]	[1.528]
∠SiSiI	107.5(10)	109.3(10)	107.2(4)	109.4(4)	107.0(10)	109.3(10)	107.2(4)	109.6(4)
∠SiSiI	107.5(10)	109.3(10)	107.2(4)	106.0(4)	107.0(10)	109.3(10)	107.2(4)	106.3(4)
∠SiSiH	[110.8]	[110.2]	[110.9]	[109.5]	[110.8]	[109.9]	[110.9]	[109.1]
∠ISiI[a]	–	–	111.7(3)	111.2(3)	–	–	111.6(3)	111.0(3)
∠ISiH[a]	109.8(5)	109.2(5)	109.9(2)	110.3(2)	110.1(5)	109.3(5)	109.9(2)	110.4(2)
V_1 (kcal mol^{-1})	0.2 ± 1.1		− 0.6 ± 1.8		–	–	–	–
V_2 (kcal mol^{-1})	[0.0]		[0.0]		–	–	–	–
V_3 (kcal mol^{-1})	1.1 ± 1.7		5.4 ± 3.3		–	–	–	–
ϕ[c]	180.0	61.1[b]	180.0	59.4[b]	180.0	49(20)	180.0	57(11)
$\alpha \times 100$[d]	40.0	60.0	22.6	77.4	30(20)	70(20)	22(23)	78(23)
ΔE_0^{G-A} (kcal mol^{-1})[e]	0.14		− 0.74		− 0.16 ± 0.65		− 0.76 ± 1.24	
R[f]	0.210		0.151		0.211		0.150	

[a] Dependent parameter.
[c] $\phi = \phi$(ISiSiI) for 1,2-diiododisilane; $\phi = \phi$(HSiSiH) for 1,1,2,2-tetraiododisilane.
[b] *Gauche* torsional angle as calculated from Eq. (5) using the obtained V_1, V_2 and V_3.
[d] Estimated conformational compositions in percent. Values for the dynamic models are appropriate sums of the contribution from the individual pseudoconformers.
[e] Conformer energy differences including entropy contributions from the vibration/rotation partition functions (the entropies were calculated from the HF/6-31G(d)/HW-ECP(I) results).
[f] The goodness of fit factor $R = [\sum w_i \Delta_i^2 / \sum w_i (s_i I_m^{exp}(s))^2]^{1/2}$ and $\Delta_i = s_i I_m^{exp}(s) - s_i I_m^{calc}(s)$.

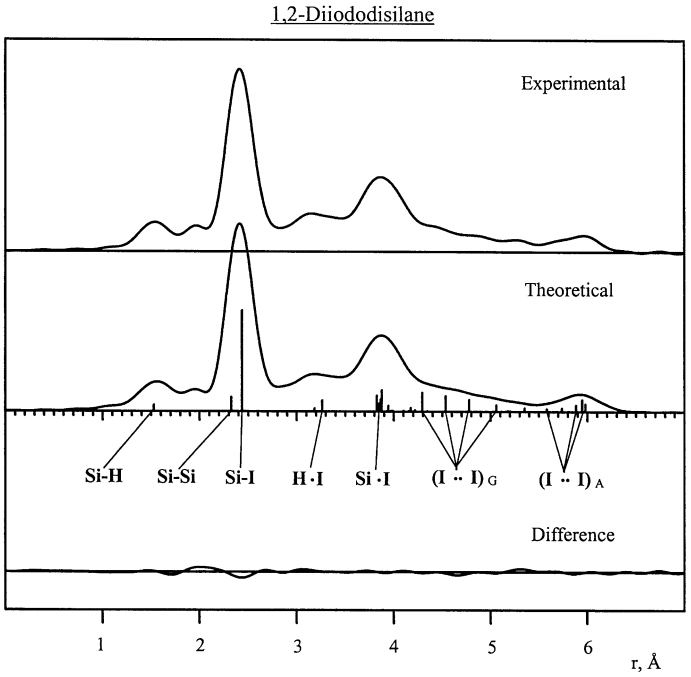

Fig. 4. Radial distribution (RD) curves for 1,2-diiododisilane. The experimental curve was calculated from the composite of the 2 average experimental curves (5 + 6) shown in Fig. 2 with the use of theoretical data for the region $0 \leq s/\text{Å}^{-1} \leq 1.75$ and $B/\text{Å}^2 = 0.0025$. The difference curve are the experimental curve minus the theoretical curve (dynamic model). The vertical lines indicate the distribution of interatomic distances according to weighted pseudoconformers, they have lengths proportional to the distance weights.

intensity curves in the form $sI_m(s)$. The average experimental intensity curves from both camera distances are shown in Fig. 2 (DIDS) and Fig. 3 (TIDS). In Fig. 4 (DIDS) and Fig. 5 (TIDS) is shown the final experimental radial distribution (RD) curves calculated in the usual way from the modified molecular intensity curves of the type $I'(s) = sI_m(s)Z_IZ_I(A_IA_I)^{-1}\exp(-0.0025s^2)$, where $A = s^2F$ and F is the absolute value of the complex electron scattering amplitudes. Theoretical intensity data were used for $s \leq 1.75$ Å^{-1} in the experimental curves before the RD curves were calculated. The scattering amplitudes and phases were taken from tables [21].

3. Structure analysis

3.1. Ab initio MO and DFT calculations

Constraints in the GED study: ab initio MO and DFT calculations were used to establish constraints in our dynamic GED models by incorporating calculated geometrical differences between the thirteen pseudoconformers as constants in the refinements. The geometries for both stable conformers of DIDS and TIDS were fully optimized using GAUSSIAN 94 [22], and the methods/basis sets: HF/6-31G(d)/HW-ECP(I) (6-31G(d) for Si and H, HW-ECP for I), HF/SBK-ECP/DZP and DFT/B3LYP/3-21G*. Geometry optimizations were also performed at the B3LYP/3-21G* level for each pseudo-form at 30° intervals from 0 to 180° for both compounds. The static (2-conformer) models were constrained using the fully optimized HF geometries.

Zero-point energies and vibrational/rotational entropies: zero-point energies (ZPE) and vibrational/rotational entropies were also estimated at the aforementioned optimized geometries using the HF/6-31G(d)/HW-ECP(I) approach. The ZPE's were found (G-A) as -0.0011 kcal mol^{-1} (DIDS) and $+0.025$ kcal mol^{-1} (TIDS). Calculated entropies

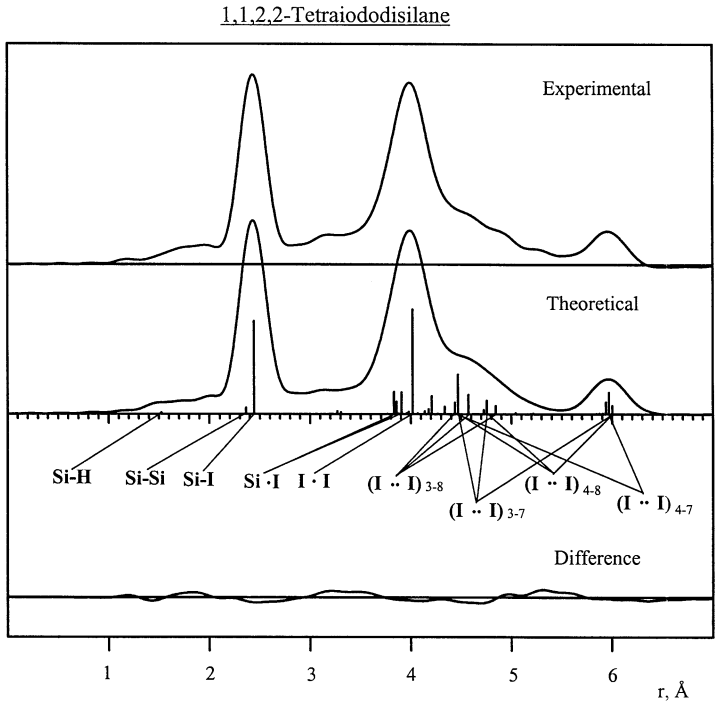

Fig. 5. Radial distribution (RD) curves for 1,1,2,2-tetraiododisilane. The experimental curve was calculated from the composite of the 2 average experimental curves (5 + 5) shown in Fig. 3 with the use of theoretical data for the region $0 \leq s/\text{Å}^{-1} \leq 1.75$ and $B/\text{Å}^2 = 0.0025$. The difference curve are the experimental curve minus the theoretical curve (dynamic model). The vertical lines indicate the distribution of interatomic distances according to weighted pseudoconformers, they have lengths proportional to the distance weights.

based purely on vibrational and rotational partition functions were $\Delta S^*_{G-A} = -0.145$ cal mol^{-1}K^{-1} (DIDS), and $\Delta S^*_{G-A} = -0.658$ cal mol^{-1}K^{-1} (TIDS). These entropy values were included when calculating experimental energy differences (ΔE_0) from the GED conformational analyses. These energy results, as well as experimental structural parameter values, are listed in Table 1.

3.2. Vibrational spectroscopy

Vibrational spectra: Tables 2 and 3 summarize the wavenumbers observed in the Raman spectra of liquid (60°C) and solid (−60°C) DIDS and TIDS, respectively. The wavenumber of the more intense lines are largely identical with those reported in [5]. A number of weak lines which are not reported in Ref. [5] have been observed due to the larger laser power available, and a number of lines could be resolved into pairs due to better experimental equipment. Two Raman lines of TIDS previously reported as 452 and 405 cm^{-1} obviously were impurities as they could not be detected in this work.

Despite a number of attempts to obtain crystalline solid samples, both disilanes formed glassy solids upon cooling which always contained both conformers, *anti* and *gauche*. Fig. 6 presents the Raman spectra of liquid and solid DIDS in the wavenumber range 70–1000 cm^{-1} illustrating the temperature dependent intensity variations that have been observed. For instance, the relative intensities within the line pairs (*anti*/*gauche*) at 339/318, 777/764 and 912/885 cm^{-1} clearly vary with temperature. Fig. 7 presents the Raman spectra for TIDS. Here also, intensity variations with temperature were observed, which are most obvious for the line pairs (*anti*/*gauche*) 310/283 and 209/214 cm^{-1}. The conformational isomers of both disilanes are outlined in Fig. 1. The molecules are composed of eight atoms giving a total of 18 normal modes. The selection rules for *anti* DIDS and *anti* TIDS predict the following distribution of the modes between the irreducible representations

Table 2
Wavenumbers ($\tilde{\nu}$) in the Raman spectra of liquid and solid $H_2ISiSiH_2I$ (DIDS)

Raman 20°C, 1 $\tilde{\nu}$/cm^{-1}	− 100°C, s $\tilde{\nu}$/cm^{-1}	IR[a] 20°C, 1 $\tilde{\nu}$/cm^{-1}	Assignment	Description
2155 vs	2157 vs	2165 vs	ν_1, ν_7, ν_{11}, ν_{14}	$\nu_{as}SiH_2$, ν_sSiH_2
912 m	908 m		ν_2	δSiH_2
		918 s	ν_{15}	δSiH_2
		904 vs	ν'_2	δSiH_2
885 m	879 m	892 s	ν'_{15}	δSiH_2
850 vw	849 vw,b	857 mw		
		805 w		
777 w	773 w		ν_3	γSiH_2
764 w,b	757 w	772s	ν'_3	γSiH_2
	720 sh	723 vs	ν'_{16}	γSiH_2
		690 vs	ν_{16}	γSiH_2
715 w,b	707 w			
674 w,b	669 w,b		ν_{12}	τSiH_2
650 w	653 w		ν'_8	τSiH_2
626 w	630 w	625 w	ν_8, ν'_{12}	τSiH_2
		520 w		
511 w,b	509 w,b		ν_{13}	ρSiH_2
495 w,b	495 w,b		ν'_9	ρSiH_2
460 m	457 m		ν_4	$\nu SiSi$
447 m	449 m		ν'_4	$\nu SiSi$
385 w	383 vw	380 mw	ν'_{13}	ρSiH_2
	361 vw,b			
		344 vs	ν_{17}	νSiI
339 s	333 s		ν_5	νSiI
		325 m	ν_9, ν'_{17}	ρSiH_2, νSiI
318 vs	313 vs		ν'_5	νSiI
285 m	282 m		$\nu'_5 - \nu'_{10}$	
168 vw	166 vw		$2\nu_6$	
129 mw,b	130 mw,b		ν'_{18}	$\delta SiSiI$
118 vw	113 vw		$2\nu'_6$	
97 w,b	95 w,b		$\nu'_6 + \nu'_{10}$	
84 s	83 s		ν_6	$\delta SiSiI$

[a] IR wavenumbers taken from Ref. [8].

of point group C_{2h}:

$$\Gamma_{vib} = 6A_g(Ra) + 4A_u(IR) + 3B_g(Ra) + 5B_u(IR) \quad (1)$$

Both molecules are centrosymmetric, and the infrared and Raman activities given in parentheses follow the rules of mutual exclusion. Table 4 summarizes the numbering and the description of the normal modes as it is used throughout the present work. The *gauche* conformers belong to point group C_2 which is a subgroup of C_{2h}. The selection rules are

$$\Gamma_{vib} = 10A(Ra, IR) + 8B(Ra, IR) \quad (2)$$

According to the correlation tables, the A_g and A_u vibrations of group C_{2h} transform into A-vibrations of point group C_2, B_g and B_u into irreducible representation B. Therefore, the numbering of the normal modes for the *anti* conformers has also been used for the *gauche* conformers. In Tables 2 and 3, the observed wavenumbers have been assigned by use of the ab initio calculations and normal coordinate analysis described later on. Primed fundamentals refer to the *gauche* conformers whenever they differ from those of the *anti* conformers.

Normal coordinate analysis (NCA): for each molecule the calculated force field (Hessian matrix) defined in Cartesian coordinates was transformed into a force field defined in non-redundant symmetry coordinates, which themselves were chosen as linear

Table 3
Wavenumbers ($\tilde{\nu}$) in the Raman spectra of liquid and solid $I_2HSiSiHI_2$ (TIDS)

Raman 20°C, 1 $\tilde{\nu}$/cm^{-1}	− 100°C, s $\tilde{\nu}$/cm^{-1}	IR[a] 20°C, 1 $\tilde{\nu}$/cm^{-1}	Assignment	Description
2158 vs	2160 vs	2165 vs	ν_1, ν_{14}	νSiH
		795 m	ν'_7	δHSiI
	762 vw,b	773 m	ν'_{11}	δHSiI
749 vw	749 w		ν_2	δSiSiH
710 vw,b			ν_{11}	δHSiI
		704 vs	ν_7	δHSiI
699 w,b	699 w,b		ν'_2	δSiSiH
685 w,b	685 w		ν'_{15}	δSiSiH
654 w,b	652 w,b			
		655 s	ν_{15}	δSiSiH
619 vw,b	618 vw,b			
481 w,b			ν_3	νSiSi
474 m	474 m	472mw	ν'_3	νSiSi
388 m	388 m	387 vs	ν_8, ν'_8, ν_{12}, ν'_{12}	$\nu_{as}SiI_2$
348 m	349 m	347 w	ν'_{16}	ν_sSiI_2
310 s	311 vs		ν_4	ν_sSiI_2
		311 ms	ν_{16}	ν_sSiI_2
283 vs	285 vs	280 m	ν'_4	ν_sSiI_2
214 m	215 s		ν'_{17}	δSiI_2
209 mw, sh	210 w		$2\nu_5$	
177 mw	178 mw		$\nu_5 + \nu_6$	
170 mw	171 mw		$2\nu_{13}$, $2\nu'_{18}$	
155 w	156 m		$\nu'_{17} - \nu'_6$	
130 s	131 s		$2\nu'_6$	
114 vs	115 vs		ν_5	δSiI_2
105 vs	105 vs		ν'_9	ρSiI_2
97 m,sh	98 m,sh		$\nu_6 + \nu_9$	
84 s	86 s		ν_{13}, ν'_{18}	ρSiI_2, γSiI_2
	78 w		$\nu_5 - \nu_9$	
65 s	66 s		ν'_6	γSiI_2
59 s	60 s		ν_6	γSiI_2

[a] IR wavenumbers taken from Ref. [8].

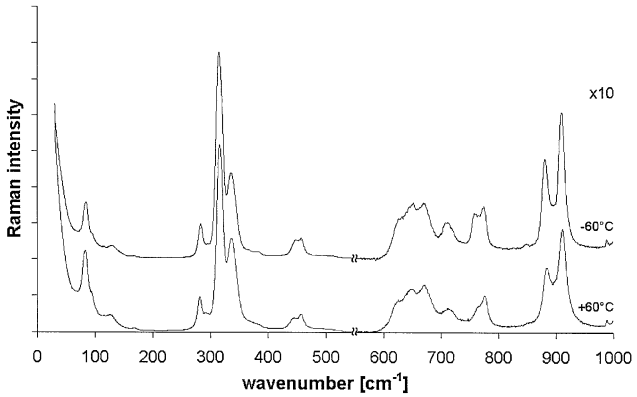

Fig. 6. Raman spectrum of liquid (+60°C) and solid (−60°C) 1,2-diiododisilane (DIDS) in the range 100–1000 cm^{-1}.

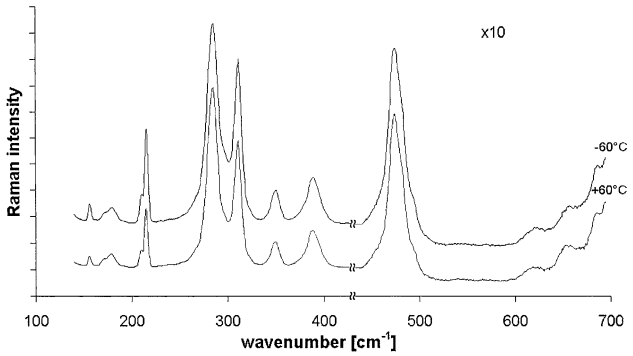

Fig. 7. Raman spectrum of liquid (+60°C) and solid (−60°C) 1,1,2,2-tetraiododisilane (TIDS) in the range 100–700 cm^{-1}.

combinations of (redundant) internal coordinates which are illustrated in Fig. 8. The definitions of the symmetry coordinates for *anti* DIDS and *anti* TIDS are compiled in Tables 5 and 6. Identical symmetry coordinates were used for the *gauche* conformers, as C_2 is a subgroup of C_{2h}. The ab initio force fields calculated at the HF/SBK-ECP/DZP [17,18] level were transformed from Cartesian coordinates to symmetry coordinates and then scaled according to the types of internal coordinates. The scale constants were: 0.89 for SiH-stretching, 0.92 for SiH-bending, 0.93 for SiSi- and SiI-stretching, 0.99 for bending involving the heavy atoms and 1.0 for the SiSi-torsion. The transformed ab initio force field, the ab initio geometry and the atomic masses were then used for the calculation of the vibrational frequencies and potential energy distributions (PED) employing the FG-method of Wilson [23]. The program ASYM40 [24,25] was used for this purpose. The results of the normal coordinate analysis, including the scaled and unscaled frequencies, the potential energy distributions and the symmetry force fields are summarized in Tables 7 and 8 for both conformers of DIDS, and in Tables 9 and 10 for *anti* and *gauche* TIDS.

Conformational isomerism: with Raman spectroscopy, enthalpy differences between conformational isomers can be determined from variable temperature spectra plotting the logarithm of intensity ratios vs. the inverse temperature by applying van't Hoff's equation

$$\ln(I_A/I_G) = -(H_A - H_G)/RT + C \quad (3)$$

I_G and I_A denote the temperature dependent intensities of vibrational bands due to the *gauche* and *anti*

Table 4
Numbering of fundamental vibrations for *anti* and *gauche* DIDS and TIDS

DIDS							TIDS						
	Anti				*Gauche*			*Anti*				*Gauche*	
Vibration	A_g	A_u	B_g	B_u	*A*	*B*	Vibration	A_g	A_u	B_g	B_u	*A*	*B*
$\nu_{as}SiH_2$		7	11		7	11	νSiH	1			14	1	14
ν_sSiH_2	1			14	1	14	δSiSiH	2			15	2	15
δSiH_2	2			15	2	15	νSiSi	3				3	
γSiH_2	3			16	3	16	δHSiI		7	11		7	11
τSiH_2		8	12		8	12	ν_sSiI_2	4			16	4	16
ρSiH_2		9	13		9	13	δSiI_2	5			17	5	17
νSiSi	4				4		γSiI_2	6			18	6	18
νSiI	5			17	5	17	$\nu_{as}SiI_2$		8	12		8	12
δSiSiI	6			18	6	18	ρSiI_2		9	13		9	13
Torsion		10			10		Torsion		10			10	

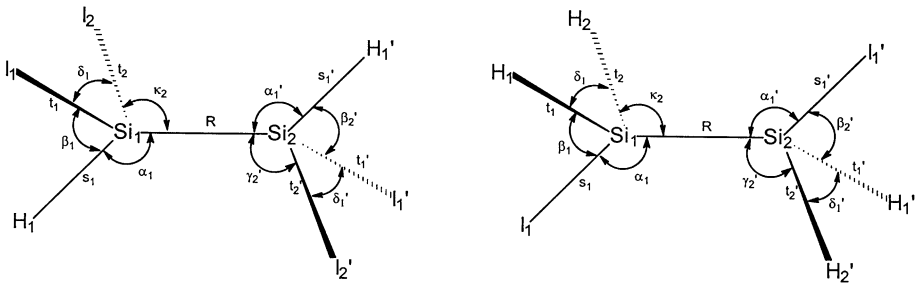

Fig. 8. Definition of the internal coordinates for TIDS (left) and DIDS (right).

conformers. For DIDS and TIDS, conformational isomerism may be expected to show up most clearly in the region of the SiH-deformations, the SiSi- and SiI-stretching vibrations and in the range of the skeleton deformations. Together, these vibrations comprise the wavenumber range 950–30 cm^{-1}. Four line pairs for DIDS and two line pairs for TIDS turned out to be suitable in performing van't Hoff analyses. These pairs, and the ΔH-values obtained from them, are summarized in Table 11, and two selected van't Hoff plots are presented in Fig. 9. For reasons described previously, the line pair 777/764 cm^{-1} of DIDS was not used for the van't Hoff analysis. Due to the inherent difficulties of the method, which are

Table 5
Symmetry coordinates (not normalized) for *anti* $I_2HSiSiHI_2$ (TIDS)

Species	No.	Description	Symmetry coordinate
A_g	S_1	νSiH	$s_1 + s'_1$
	S_2	δSiSiH	$5\alpha_1 - \beta_1 - \beta_2 - \gamma_1 - \gamma_1 - \delta_1 + 5\alpha'_1 - \beta'_1 - \beta'_2 - \gamma'_1 - \gamma'_1 - \delta'_1$
	S_3	νSiSi	R
	S_4	$\nu_s SiI_2$	$t_1 + t_2 + t'_1 + t'_2$
	S_5	δSiI_2	$4\delta_1 - \beta_1 - \beta_2 - \gamma_1 - \gamma_2 + 4\delta'_1 - \beta'_1 - \beta'_2 - \gamma'_1 - \gamma'_2$
	S_6	γSiI_2	$\beta_1 + \beta_2 - \gamma_1 - \gamma_2 + \beta'_1 + \beta'_2 - \gamma'_1 - \gamma'_2$
A_u	S_7	δHSiI	$\beta_1 - \beta_2 + \gamma_1 - \gamma_2 + \beta'_1 - \beta'_2 + \gamma'_1 - \gamma'_2$
	S_8	$\nu_{as} SiI_2$	$t_1 - t_2 - t'_1 + t'_2$
	S_9	ρSiI_2	$\beta_1 - \beta_2 - \gamma_1 + \gamma_2 + \beta'_1 - \beta'_2 - \gamma'_1 + \gamma'_2$
	S_{10}	Torsion	$\tau_1 + \tau_2 + \tau_3 + \tau_4 + \tau_5 + \tau_6 + \tau_7 + \tau_8 + \tau_9$
B_g	S_{11}	δHSiI	$\beta_1 - \beta_2 + \gamma_1 - \gamma_2 - \beta'_1 + \beta'_2 - \gamma'_1 + \gamma'_2$
	S_{12}	$\nu_{as} SiI_2$	$t_1 - t_2 + t'_1 - t'_2$
	S_{13}	ρSiI_2	$\beta_1 - \beta_2 - \gamma_1 + \gamma_2 - \beta'_1 + \beta'_2 + \gamma'_1 - \gamma'_2$
B_u	S_{14}	νSiH	$s_1 - s'_1$
	S_{15}	δSiSiH	$5\alpha_1 - \beta_1 - \beta_2 - \gamma_1 - \gamma_2 - \delta_1 - 5\alpha'_1 + \beta'_1 + \beta'_2 + \gamma'_1 + \gamma'_2 + \delta'_1$
	S_{16}	$\nu_s SiI_2$	$t_1 + t_2 - t'_1 - t'_2$
	S_{17}	δSiI_2	$4\delta_1 - \beta_1 - \beta_2 - \gamma_1 - \gamma_2 - 4\delta'_1 + \beta'_1 + \beta'_2 + \gamma'_1 + \gamma'_2$
	S_{18}	γSiI_2	$\beta_1 + \beta_2 - \gamma_1 - \gamma_2 - \beta'_1 - \beta'_2 + \gamma'_1 + \gamma'_2$

Table 6
Symmetry coordinates (not normalized) for *anti* IH_2SiSiH_2I (DIDS)

Species	no.	Description	Symmetry coordinate
A_g	S_1	$\nu_s SiH_2$	$t_1 + t_2 + t'_1 + t'_2$
	S_2	δSiH_2	$4\delta_1 - \beta_1 - \beta_2 - \gamma_1 - \gamma_2 + 4\delta'_1 - \beta'_1 - \beta'_2 - \gamma'_1 - \gamma'_2$
	S_3	γSiH_2	$\beta_1 + \beta_2 - \gamma_1 - \gamma_2 + \beta'_1 + \beta'_2 - \gamma'_1 - \gamma'_2$
	S_4	$\nu SiSi$	R
	S_5	νSiI	$s_1 + s'_1$
	S_6	$\delta SiSiI$	$5\alpha_1 - \beta_1 - \beta_2 - \gamma_1 - \gamma_1 - \delta_1 + 5\alpha'_1 - \beta'_1 - \beta'_2 - \gamma'_1 - \gamma'_1 - \delta'_1$
A_u	S_7	$\nu_{as} SiH_2$	$t_1 - t_2 - t'_1 + t'_2$
	S_8	τSiH_2	$\beta_1 - \beta_2 - \gamma_1 + \gamma_2 + \beta'_1 - \beta'_2 - \gamma'_1 + \gamma'_2$
	S_9	ρSiH_2	$\beta_1 - \beta_2 + \gamma_1 - \gamma_2 + \beta'_1 - \beta'_2 + \gamma'_1 - \gamma'_2$
	S_{10}	Torsion	$\tau_1 + \tau_2 + \tau_3 + \tau_4 + \tau_5 + \tau_6 + \tau_7 + \tau_8 + \tau_9$
B_g	S_{11}	$\nu_{as} SiH_2$	$t_1 - t_2 + t'_1 - t'_2$
	S_{12}	τSiH_2	$\beta_1 - \beta_2 - \gamma_1 + \gamma_2 - \beta'_1 + \beta'_2 + \gamma'_1 - \gamma'_2$
	S_{13}	ρSiH_2	$\beta_1 - \beta_2 + \gamma_1 - \gamma_2 - \beta'_1 + \beta'_2 - \gamma'_1 + \gamma'_2$
B_u	S_{14}	$\nu_s SiH_2$	$t_1 + t_2 - t'_1 - t'_2$
	S_{15}	δSiH_2	$4\delta_1 - \beta_1 - \beta_2 - \gamma_1 - \gamma_2 - 4\delta'_1 + \beta'_1 + \beta'_2 + \gamma'_1 + \gamma'_2$
	S_{16}	γSiH_2	$\beta_1 + \beta_2 - \gamma_1 - \gamma_2 - \beta'_1 - \beta'_2 + \gamma'_1 + \gamma'_2$
	S_{17}	νSiI	$s_1 - s'_1$
	S_{18}	$\delta SiSiI$	$5\alpha_1 - \beta_1 - \beta_2 - \gamma_1 - \gamma_2 - \delta_1 - 5\alpha'_1 + \beta'_1 + \beta'_2 + \gamma'_1 + \gamma'_2 + \delta'_1$

described thoroughly in an excellent review by P. Klaboe [26], individual ΔH-values may differ by a factor of up to five, or even more. By taking *mean values* from Table 11, ΔH_{G-A}-values of -0.31 ± 0.14 and -0.14 ± 0.10 kcal mol^{-1} are obtained for DIDS and TIDS, respectively. For both disilanes, the low energy conformer clearly is *gauche* in the liquid state. This conclusion is independent of some ambiguities in the assignments of fundamentals.

3.3. Gas electron diffraction

Details of the dynamic model: the GED data were treated by fitting a three-term cosine potential function to the experimental data. The cosine potential

$$V(\phi) = \frac{1}{2} \sum_i V_i[1 - \cos i(180 - \theta)] \quad (4)$$

with $i = 1$–3; $\phi = \phi$(ISiSiI) for DIDS, and $\phi = \phi$(HSiSiH) for TIDS, was obtained by using pseudoconformers, each one representative of a finite displacement of the large-amplitude torsional coordinate, and each given a weight determined by Boltzmann statistics in which the cosine potential $V(\phi)$ appeared as the energy factor [27]. The cosine potential function $V(\phi)$ has the property that $V(180°) = 0$, $V(0°) = V_1 + V_3$, and $V(60°) = (3/4)(V_1 + V_2)$. By using pseudoconformers at 15° intervals from syn (0°) to *anti* (180°), comprising a total of 13 pseudoconformers, refined values for V_1 and V_3 were obtained simultanously, and from these values the experimental torsional potential curve for the rotation around the Si–Si bond could be calculated. In addition, static 2-conformer models were constructed for both molecules, with slightly different treatment of shrinkage, giving independent sets of results making it possible to check the consistency in the experimental data; cf. Table 1. It was shown previously

Table 7
Calculated and observed wavenumbers ($\tilde{\nu}$), potential energy distributions (contributions from diagonal elements, >10%) and symmetry force constants (deformation constants weighted by 100 pm) for *anti* DIDS

		Ab initio		Exp.		PED/%	F_{ij}/N cm^{-1} [b]					
Species	ν_i	$\tilde{\nu}$/cm^{-1} [a]	$\tilde{\nu}$/cm^{-1} [b]	Ra $\tilde{\nu}$/cm^{-1}	Ir $\tilde{\nu}$/cm^{-1} [c]							
A_g	1	2291	2161	2155		100(1)	2.71	0.05	− 0.04	0.02	0.04	− 0.05
	2	963	924	912		94(2)		0.42	0	− 0.03	− 0.07	− 0.04
	3	839	804	777		97(3)			0.54	− 0.07	0.16	0
	4	479	461	460		87(4)				1.75	0.03	− 0.04
	5	363	352	339		86(5), 27(6)					1.83	0.16
	6	85	84	84		75(6), 11(5)						0.55
A_u	7	2315	2184		2165	100(7)	2.70	− 0.03	0.02	0		
	8	645	619		625	79(8)		0.31	0.12	0		
	9	350	335		325	114(9), 39(8)			0.34	0		
	10	33	33			95(10)				0.005		
B_g	11	2306	2175	2155		100(11)	2.69	− 0.04	0.07			
	12	714	685	674		97(12)		0.41	− 0.02			
	13	533	511	511		99(13)			0.50			
B_u	14	2289	2160		2165	100(14)	2.71	0.06	0	0.01	− 0.03	
	15	954	915		918	100(15)		0.42	− 0.03	− 0.04	− 0.06	
	16	734	704		690	101(16)			0.41	0.15	− 0.10	
	17	363	350		344	102(17)				1.77	0.01	
	18	55	55		–	116(18), 14(16)					0.26	

[b] Scaled HF/SBK-ECP/DZP calculations according to Section 3.2.
[a] Unscaled HF/SBK-ECP/DZP calculations.
[c] Infrared wavenumbers from Ref. [8].

[1] that the *gauche* torsional angle ϕ_G may be written:

$$\phi_G = 180 - \cos^{-1}\left(\frac{-4V_2 - \sqrt{16V_2^2 - 48V_3(V_1 - 3V_3)}}{24V_3}\right) \quad (5)$$

with $V_3 \neq 0$. Eq. (5) gives the relation between the *gauche* minimum torsional angle and the obtained potential parameters V_i, $i = 1$–3.

Refinements and normal coordinate calculations: refinements of the molecular structures based on the GED data were made by the least-squares method [28], adjusting a theoretical $sI_m(s)$ curve simultaneously to the eleven (DIDS) and ten (TIDS) experimental intensity curves, one from each of the photographic plates, using a unit weight matrix. The structures were converted from the geometrically consistent r_α to the r_a-type required by the formula for the theoretical scattered intensities ($r_a = r_g - \mathcal{L}^2/r = r_\alpha - \mathcal{L}^2/r + K_T + \delta r$) [29,30], by using values of the centrifugal distortion constants (δr), perpendicular amplitude corrections (K_T) and root-mean-square amplitudes of vibration ($\mathcal{L}$) calculated at the temperatures of the experiments, 328 K (DIDS) and 428 K (TIDS). These vibrational quantities were estimated from the ab initio Cartesian force fields (HF/6-31G(d)/HW-ECP(I)) as previously described under the spectroscopy section. A set of scale factors for the nonredundant set of symmetry force constants for each conformer of each molecule was then refined to fit the observed vibrational wavenumbers for two isotopomers in both cases. The experimental wavenumbers are presented in Tables 7 and 8 for DIDS, and Tables 9 and 10 for TIDS. The resulting SQM force fields were used to calculate the vibrational amplitudes and corrections previously described, including all pseudo-conformers comprised by the dynamic model by using the obtained B3LYP/3-21G* optimized geometries.

Table 8
Calculated and observed wavenumbers ($\tilde{\nu}$), potential energy distributions (contributions from diagonal elements, >10%) and symmetry force constants (deformation constants weighted by 100 pm) for *gauche* DIDS

		Ab initio		Exp.		PED/%	F_{ij}/N cm^{-1}[b]									
Species	ν_i	$\tilde{\nu}$/cm^{-1}[a]	$\tilde{\nu}$/cm^{-1}[b]	Ra $\tilde{\nu}$/cm^{-1}	Ir $\tilde{\nu}$/cm^{-1}[c]											
A	1	2282	2153	2155	2165	91(1)	2.70	0.04	0	−0.04	0.03	−0.03	0.01	0	0.01	0
	2	972	932	912	904	98(2)		0.44	−0.03	−0.03	0.12	−0.06	0	0	−0.01	0
	3	823	789	764	772	89(3)			0.49	0.02	−0.06	−0.08	−0.01	0.04	−0.04	0
	4	466	448	447	–	58(4), 19(9)				1.72	0.04	0.04	−0.01	−0.01	0.03	0
	5	330	318	318	325	77(5), 19(4)					1.86	0.08	0	0.02	−0.04	0
	6	68	68	–	–	112(6), 27(10)						0.43	−0.02	0.10	−0.08	0.01
	7	2301	2171	2155	2165	91(7)							2.67	−0.04	0.06	0
	8	679	651	650	–	93(8)								0.37	0.03	0
	9	512	493	495	495	74(9), 17(4)									0.47	0
	10	23	23	–	–	77(19)										0.01
B	11	2306	2176	2155	2165	87(11), 11(14)	2.68	−0.04	0.04	0.02	0	0.01	0	0.03		
	12	650	624	626	625	85(12)		0.33	0.09	0	0	−0.04	−0.03	−0.08		
	13	433	418	385	380	79(13), 11(12)			0.39	−0.01	0	0.04	0.04	0.09		
	14	2275	2146	2155	2165	88(14), 12(11)				2.69	0.06	0	0.01	−0.05		
	15	945	906	885	892	100(15)					0.42	−0.02	−0.05	−0.05		
	16	778	746	715	723	95(16)						0.44	0.20	0		
	17	351	338	318	325	89(17), 16(13)							1.82	0.10		
	18	125	124	129	–	107(18), 11(12), 18(13)								0.49		

[b] Scaled HF/SBK-ECP/DZP calculations according to Section 3.2.
[a] Unscaled HF/SBK-ECP/DZP calculations.
[c] Infrared wavenumbers from Ref. [8].

Table 9
Calculated and observed wavenumbers ($\tilde{\nu}$), potential energy distributions (contributions from diagonal elements, >10%) and symmetry force constants (deformation constants weighted by 100 pm) for *anti* TIDS

		Ab initio		Exp.		PED/%	F_{ij}/N cm^{-1}[b]					
Species	ν_i	$\tilde{\nu}$/cm^{-1}[a]	$\tilde{\nu}$/cm^{-1}[b]	Ra $\tilde{\nu}$/cm^{-1}	Ir $\tilde{\nu}$/cm^{-1}[c]							
A_g	1	2288	2159	2158		100(1)	2.68	0.06	0	0.02	0.02	−0.01
	2	795	768	749		84(2), 21(5)		0.50	0.05	−0.13	0.01	−0.07
	3	495	479	481		79(3), 14(4)			1.70	0.04	−0.03	−0.07
	4	328	317	310		57(4), 35(5)				1.95	−0.04	0.06
	5	116	114	114		30(5), 29(4), 20(6)					0.63	0.07
	6	57	57	59		70(6), 15(5)						0.63
A_u	7	738	721		704	59(7), 44(9)	0.49	0.17	0.01	0.04		
	8	410	396		387	102(8)		1.72	0	0		
	9	35	34		–	35(9), 43(7)			0.38	−0.02		
	10	12	12		–	189(10)				0.01		
B_g	11	737	717	710		67(11), 44(13)	0.55	0.28	−0.03			
	12	411	396	388		100(12), 14(11)		1.71	−0.05			
	13	83	81	84		49(13), 27(12)			0.01			
B_u	14	2291	2162		2165	100(14)	2.68	0.02	0	0.02	0.01	
	15	651	633		655	57(15), 28(17)		0.25	−0.10	−0.08	−0.09	
	16	325	317		311	94(16), 14(18)			1.86	0.08	0.10	
	17	92	91		–	79(17), 57(15)				0.49	−0.02	
	18	87	86		–	84(18)					0.57	

[b] Scaled HF/SBK-ECP/DZP calculations according to Section 3.2.
[a] Unscaled HF/SBK-ECP/DZP calculations.
[c] Infrared wavenumbers from Ref. [8].

The GED molecular parameters: the geometry of each of the conformers of the two molecules can be described by a set of independent parameters which were fitted to the experimental data. In our refinements these parameters were chosen as r(Si–Si), r(Si–I), r(Si–H), ∠(SiSiH), ∠(SiSiI), P(ISiI) (projection angle for TIDS; the angle between the two Si–I bonds projected on a plane perpendicular to the Si–Si-bond), P(HSiH) (similar projection angle for DIDS), the torsional angle parameter ϕ(XSiSiX) (in increments of 15°; X = I for DIDS, X = H for TIDS); along with the three potential constants V_1, V_2, V_3 and several difference parameters held at constant values. Ab initio constraints were incorporated into these difference parameters as described earlier. The r(Si–H) parameter value could not be refined and was held constant in the least squares refinements, and the r_α value used was calculated from the assumed r_e ab initio value (B3LYP/3-21G*) by using the anharmonicity constant $a_3 = 2.0$ Å^{-1} [31] in the usual formula $r_\alpha = r_e + 3a_3\ell^2/2$. Many, but not all, of the amplitudes could successfully be refined. In the final refinements three geometrical parameters, three amplitude parameters and the two potential constants (V_i; $i = 1,3$) were refined simultaneously for both DIDS and TIDS. The results of these refinements are given in Table 1. In Table 12 the present results for these molecules are compared with the previous GED results from 1991 [4], 1,1,2-triiododisilane [1], and also with results for iodosilane ($IH_2Si–SiH_3$; MW) [12]. In Table 13 an overview of the obtained conformer compositions for the iododisilanes are shown. In Table 14 the HF MO- and DFT calculations have been assembled. In Tables 15 and 16 selected experimental bond distances for DIDS and TIDS are shown, together with the corresponding distances obtained from the DFT calculations, as well as theoretical and experimental vibrational amplitudes (ℓ_{ij}). The theoretical intensity curves for the final models (dynamic type) are shown in Figs. 2 and 3 for DIDS and TIDS, respectively, together with average experimental and difference curves. The corresponding RD

Table 10
Calculated and observed wavenumbers ($\tilde{\nu}$), potential energy distributions (contributions from diagonal elements, >10%) and symmetry force constants (deformation constants weighted by 100 pm) for *gauche* TIDS

		Ab initio		Exp.		PED/%	F_{ij}/N cm^{-1} [b]								
Species	ν_i	$\tilde{\nu}$/cm^{-1} [a]	$\tilde{\nu}$/cm^{-1} [b]	Ra $\tilde{\nu}$/cm^{-1}	Ir $\tilde{\nu}$/cm^{-1} [c]										
A	1	2283	2154	2158	2165	100(1)	2.66	0.04	0.01	0.02	0.01	0	− 0.02	0	0.01	0
	2	725	705	699	–	49(2), 23(5), 14(7), 13(9)		0.36	0	− 0.09	− 0.04	− 0.09	− 0.07	− 0.05	0.04	0
	3	491	475	474	472	69(3), 18(4)			1.68	0.04	− 0.08	− 0.02	− 0.05	− 0.01	0.04	0
	4	290	281	283	280	59(4), 15(3), 10(5)				1.96	− 0.02	0.05	0.03	− 0.02	− 0.02	0
	5	40	39	–	–	41(5),30(2),10(6),20(7),18(9)					0.65	0.02	− 0.01	− 0.03	0	0
	6	62	62	65	–	55(6), 13(7), 18(9)						0.57	− 0.01	0.01	0.01	0
	7	758	736	762	795	46(7), 15(2), 34(9)							0.48	0.24	− 0.02	0
	8	409	395	388	387	97(8)								1.73	− 0.03	0
	9	109	106	105	–	12(9), 20(4), 16(5), 25(6)									0.44	0.01
	10	15	15	–	–	100(10)										0.01
B	11	752	732		773	47(11), 39(13)	0.43	0.19	0.03	0.02	0.07	− 0.03	0.04	0.04		
	12	413	399	388	387	100(12)		1.73	0	0	0.05	− 0.02	0.03	− 0.01		
	13	35	34	–	–	55(13), 53(11)			0.39	− 0.01	− 0.07	0.02	− 0.03	− 0.02		
	14	2280	2151	2158	2165	100(14)				2.66	0.04	0	0.03	0		
	15	704	682	685	–	76(15), 22(17)					0.40	− 0.16	0.02	− 0.08		
	16	334	324	348	347	84(16), 11(18)						1.88	0.04	0.09		
	17	188	186	214	–	58(17), 12(16)							0.56	− 0.02		
	18	85	84	84	–	89(18)								0.55		

[b] Scaled HF/SBK-ECP/DZP calculations according to Section 3.2.
[a] Unscaled HF/SBK-ECP/DZP calculations.
[c] Infrared wavenumbers from Ref. [8].

Table 11
ΔH-values obtained for various line pairs of DIDS and TIDS

DIDS			TIDS		
Line pair (A/G)	$H_A - H_G$ (kcal mol^{-1})	$H_A - H_G$ (kJ mol^{-1})	Line pair (A/G)	$H_A - H_G$ (kcal mol^{-1})	$H_A - H_G$ (kJ mol^{-1})
84/118	0.23	0.98	209/214	0.06	0.24
339/318	0.22	0.90	310/283	0.23	0.98
460/447	0.45	1.90			
912/885	0.34	1.41			
Average:	0.31	1.30		0.14	0.61

curves along with the difference curves are shown in Figs. 4 and 5 for DIDS and TIDS, respectively.

4. Discussion

Taking the alkanes as a reference point, many 1,2-disubstituted haloethanes have been studied, both in the gas and liquid phases [32,33]. When halogens are substituents in alkanes, factors other than steric repulsion have been found to be important in the conformational choice, such as dipole orientation and van der Waals interaction, because of the greater polarizability of non-bonding electrons on the higher halogens. Dipole association has been invoked to explain the stabilization of *gauche* conformers [33]. Recently it has been convincingly shown by Weinhold and co-workers that the primary contributions to the barrier in ethane-like molecules arise from vicinal interactions between orbitals of bond and antibond type [34,35]. This analysis is closely related to the concept of 'second order hyperconjugation', as proposed by Mulliken [36,37]. The part of the barrier that is exclusively due to vicinal bond–antibond interactions has been referred to as 'intrinsic barrier', it can be calculated by deletion of bond–antibond matrix

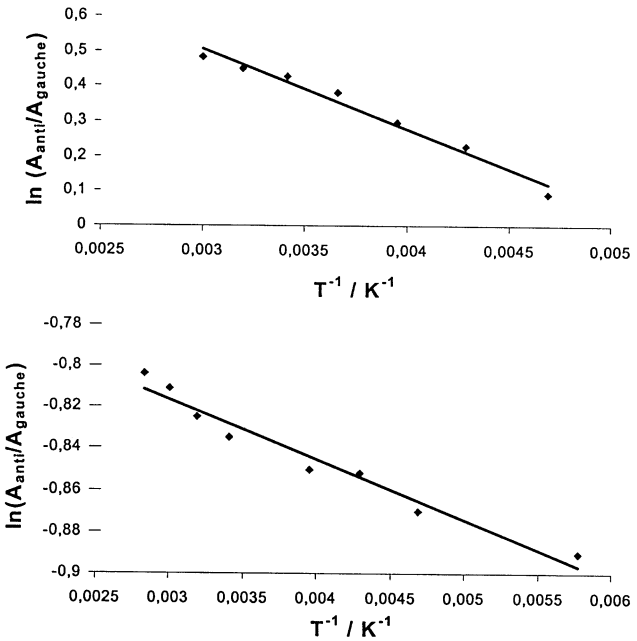

Fig. 9. Van't Hoff plots for the line pair 339/318 cm^{-1} of DIDS (top) and the line pair 310/283 cm^{-1} of TIDS (bottom).

Table 12
Comparison of results from GED investigations (r_g, $\angle_\alpha$) and MW (r_0) of some related iododisilanes (Distances are in ångstrøms (Å), angles ($\angle_\alpha$) in degrees) (X = I)

Parameter:	$IH_2Si–SiH_2I$ (1991)	$I_2HSi–SiHI_2$ (1991)	$IH_2Si–SiH_2I$ (*anti* values)	$I_2HSi–SiHI_2$ (*anti* values)	$I_2HSi–SiH_2I$	$IH_2Si–SiH_3$ (MW)
r(Si–Si)	2.380(34)	2.389(37)	2.315(26)	2.364(30)	2.329(12)	2.336(9)
r(Si–X)	2.429(13)	2.440(9)	2.447(6)	2.450(6)	2.449(3)	2.440(9)
r(Si–H)	1.510(25)	1.50[a]	1.528[a]	1.531[a]	1.527[a]	1.485(9)
∠SiSiX	107.5(12)	107.2(10)	107.5(10)	107.2(4)	109.9(4)	106.7(3)
∠XsiX	–	111.4(6)	–	111.7(3)	110.5(4)	
∠SiSiH	111.9(157)	111.9[a]	110.8[a]	110.9[a]	110.1[a]	111.5(18)
∠XsiH	107.9(170)	109.6(8)	109.8(5)	109.9(2)	109.0(2)	
$r(X\cdots X)_{anti}$	5.97	5.97	5.98	6.00	6.01	
$r(X\cdots X)_{gauche}$	4.41	4.45	4.56	4.46	4.57	
$\phi(anti)$[b]	180	180	180	180	180	
$\phi(gauche)$[b]	58(31)	61(27)	61.1[d]	59.4[d]	80[d]	
$\alpha \times 100$ (*gauche*)[c]	76(16)	60(29)	60	77	49	
Reference:	[4]	[4]	Present work	Present work	[1]	[12]

[a] Assumed, estimated or theoretical value.
[b] Torsion angles. For *anti* a C_{2h} (C_s for $I_2HSi–SiH_2I$) symmetry was assumed, with torsion angles of exactly 180°.
[d] Calculated from Eq. (5) using the refined V_1, V_2, V_3 parameters, as explained in the text.
[c] Estimated percentage of the *gauche* conformer observed in the gas phase.

Table 13
Estimated conformational compositions (%) of 1,2-diiododisilane (DIDS) and 1,1,2,2-tetraiododisilane (TIDS) as obtained from various theoretical and physical methods (Energy values in kcal mol^{-1}. All compositions estimated by using simple Boltzmann statistics, calculated at the temperatures of the GED experiments (55 and 155°C for DIDS and TIDS, respectively))

	GED (present work) [a]		HF/6-31G(d)/HW-ECP(I)		B3LYP/3-21G*		MM[b]		Raman var. temp. [c]	
	DIDS	TIDS	DIDS	TIDS	DIDS	TIDS	DIDS	TIDS	DIDS	TIDS
Conformer:										
Anti:	40	23	72	37	76	44	20	21	24	30
Gauche:	60	77	28	63	24	56	80	79	76	70

[a] Values obtained using the cosine potential function described in Section 3.3.
[b] Values obtained by molecular-mechanics (MM) calculations from Ref. [45].
[c] Compositions derived from the average values obtained from the temperature-dependent Raman spectra (present work; cf. Table 11).

Table 14
Calculated molecular parameters and relative energies for 1,2-diiododisilane and 1,1,2,2-tetraiododisilane (For atom numbering, cf. Fig. 1)

	1,2-diiododisilane				1,1,2,2-tetraiododisilane			
Method/basis set:	B3LYP/3-21G*		HF/6-31G(d)/HW-ECP(I)		B3LYP/3-21G*		HF/6-31G(d)/HW-ECP(I)	
r(DIDS/TIDS):	*Anti*	*Gauche*	*Anti*	*Gauche*	*Anti*	*Gauche*	*Anti*	*Gauche*
r(Si–Si)	2.321	2.329	2.342	2.347	2.327	2.328	2.355	2.353
$r(Si–I_{2,6}/Si–H_{2,6})$	2.474	2.469	2.495	2.487	1.482	1.483	1.463	1.465
$r(Si–H_{3,8}/Si–I_{3,8})$	1.484	1.487	1.468	1.471	2.466	2.456	2.478	2.470
$r(Si–H_{4,7}/Si–I_{4,7})$	1.484	1.484	1.468	1.468	2.466	2.468	2.478	2.479
$\angle SiSiI_{2,6}/ SiSiH_{2,6}$	108.2	109.8	108.6	111.0	110.9	110.1	111.1	109.2
$\angle SiSiH_{3,8}/ SiSiI_{3,8}$	110.8	109.9	111.4	109.7	108.7	110.4	109.8	112.2
$\angle SiSiH_{4,7}/ SiSiI_{4,7}$	110.8	110.6	111.4	111.3	108.7	107.5	109.8	108.9
∠IsiI	–	–	–	–	111.7	113.4	110.9	112.1
∠ISiH	108.7	108.6	107.3	107.3	108.4	107.7	107.6	107.1
ϕ(2-1-5-6) [a]	180.0	66.0	180.0	71.2	180.0	67.9	180.0	66.7
ΔE_0 (kcal mol^{-1})[b]	0.0	1.22	0.0	1.06	0.0	0.38	0.0	0.13
$\alpha \times 100$[c]	76.5	23.5	71.8	28.2	43.9	56.1	36.8	63.2

[a] Torsion angles.
[b] Conformational energy differences including scaled ZPE corrections.
[c] Conformational compositions (%) calculated by simple Boltzmann statistics.

elements in the Fock matrix expressed in the natural bond orbital (NBO) basis [34,35,38,39]. The Weinhold NBO picture correctly describes the conformational behaviour of numerous ethane-like molecules. For instance, the fact that the *gauche* conformer of 1,2-difluoroethane is more stable than the *anti* [40] (the *gauche effect*) can be explained by the fact that the hyperconjugative donation from a σCH bond into a trans σ*CF antibond is more stabilizing than the donation from a σCF bond into a trans σ*CF antibond [40,41]. The *energy lowering* δE_σ of a bond orbital σ due to its interaction with a vicinal antibond σ* can be estimated from second order perturbation theory as

$$\delta E_\sigma \approx H_{\sigma\sigma}^2/(H_{\sigma^*\sigma^*} - H_{\sigma\sigma}) \quad (6)$$

In a crude model it is assumed that the total intrinsic barrier contains additive contributions from vicinal bond–antibond interactions which are calculated by the formula given above. However, the influence of competing electrostatic and steric interactions on rotational barriers in ethane-like molecules need not be negligible. For example, 1-chloro-2-fluoroethane prefers the *anti* conformation in the gas phase although the predicted intrinsic barrier favours *gauche* [42].

To obtain a qualitative picture of the relevant bond–antibond interactions for the iododisilanes, NBO analyses using HF wave functions were performed for DIDS and TIDS. The calculations of intrinsic barriers and vicinal σ/σ* interactions employed geometries with constant bond lengths and bond angles, allowing us to calculate bond antibond interactions as a function of the bond antibond dihedral angle. Fig. 10 displays the vicinal bond antibond interaction energies σSiIσ*SiI, σSiIσ*SiH, σSiHσ*SiI and σSiHσ*SiH for DIDS as a function of the dihedral angle between the bonds. All of the predicted bond–antibond interaction energies display maxima (i.e. higher stability) for dihedral angles of 180°, and two of them (σSiHσ*SiH and σSiIσ*SiH) also noticeable maxima at 0°. At 180°, the interaction energies σSiIσ*SiI and σSiHσ*SiI differ very little (1.73 vs. 1.65 kcal mol^{-1}). Summing up all interaction energies gives a qualitative picture of the intrinsic barrier, which is shown in Fig. 11 together with the total barrier predicted by the HF calculations. The intrinsic barrier gives no preference for either the *gauche* or the *anti* conformer as there is no best

Table 15
Interatomic distances and vibrational amplitudes for 1,2-diiododisilane, along with corresponding B3LYP/3-21G* distances. Experimental GED values taken were from the dynamic model refinements (Distances (r) and vibrational amplitudes (ℓ) are in ångstrøms (Å))

	GED				DFT
	1,2-Diiododisilane				B3LYP/3-21G*
	r_α	r_g	ℓ_{exp}	ℓ_{calc}	r_e
Bonding (anti values)					
Si–Si	2.310(26)	2.315	0.058(19)[a]	0.060	2.321
Si–I	2.432(6)	2.447	0.056(19)[a]	0.057	2.474
Si–H	[1.508]	[1.528]	–	0.089	1.483
Torsion independent (anti values)					
$H_3\cdots H_4$	[2.441]	[2.465]	–	0.152	2.424
$H_7\cdots H_8$	[2.441]	[2.465]	–	0.152	2.424
$H_3\cdots I_2$	3.267(10)	3.286	–	0.144	3.268
$H_7\cdots I_6$	3.267(10)	3.286	–	0.144	3.268
$H_4\cdots I_2$	3.267(10)	3.286	–	0.144	3.268
$H_8\cdots I_6$	3.267(10)	3.286	–	0.144	3.268
$Si_5\cdots I_2$	3.826(20)	3.834	0.173(13)[b]	0.164	3.885
$Si_1\cdots I_6$	3.826(20)	3.834	0.173(13)[b]	0.164	3.885
$Si_1\cdots H_7$	3.176(23)	3.186	–	0.155	3.168
$Si_5\cdots H_3$	3.176(23)	3.186	–	0.155	3.168
$Si_1\cdots H_8$	3.176(23)	3.186	–	0.155	3.168
$Si_5\cdots H_4$	3.176(23)	3.186	–	0.155	3.168
Torsion dependent anti conformer					
$I_2\cdots I_6$	5.981(27)	5.984	0.161(59)[c]	0.130	6.085
$H_7\cdots I_2$	4.111(25)	4.121	–	0.285	4.169
$H_4\cdots I_6$	4.111(25)	4.121	–	0.285	4.169
$H_8\cdots I_2$	4.111(25)	4.121	–	0.285	4.169
$H_3\cdots I_6$	4.111(25)	4.121	–	0.285	4.169
$H_3\cdots H_7$	4.402(20)	4.416	–	0.164	4.369
$H_4\cdots H_8$	4.402(20)	4.416	–	0.164	4.369
$H_3\cdots H_8$	3.663(24)	3.675	–	0.256	3.635
$H_4\cdots H_7$	3.663(24)	3.675	–	0.256	3.635
Gauche conformer					
$I_2\cdots I_6$	4.539(55)	4.555	0.302(60)[c]	0.271	4.632
$H_7\cdots I_2$	4.157(25)	4.173	–	0.279	4.205
$H_4\cdots I_6$	4.157(25)	4.173	–	0.279	4.205
$H_8\cdots I_2$	5.195(15)	5.205	–	0.147	5.230
$H_3\cdots I_6$	5.195(15)	5.205	–	0.147	5.230
$H_3\cdots H_7$	3.648(24)	3.662	–	0.239	3.629
$H_4\cdots H_8$	3.648(24)	3.662	–	0.239	3.629
$H_3\cdots H_8$	3.642(24)	3.650	–	0.254	3.639
$H_4\cdots H_7$	4.398(20)	4.420	–	0.162	4.365

[a–c] These vibrational amplitudes were refined in groups.

σ-donor bond which can be placed *anti* to the best σ-acceptor bond. One approach to rationalize the importance of the dipole dipole repulsion is to examine the I–Si–Si–I dihedral angle of the *gauche* conformer. This angle should be less than the idealized value of 60° if there is electrostatic attraction, and greater than 60° if there is repulsion. The experimental value of $\phi_G \approx 60°$ (cf. Table 1) supports the argument that it is

Table 16
Interatomic distances and vibrational amplitudes for 1,1,2,2-tetraiododisilane, along with corresponding B3LYP/3-21G* distances. Experimental GED values were taken from the dynamic model refinements (Distances (r) and vibrational amplitudes (ℓ) are in ångstrøms (Å))

	GED				DFT
	1,1,2,2-tetraiododisilane				B3LYP/3-21G*
	r_α	r_g	ℓ_{exp}	ℓ_{calc}	R_e
Bonding (anti values)					
Si–Si	2.356(30)	2.364	0.061(9)[a]	0.065	2.327
Si–$I_{3,8}$	2.433(6)	2.450	0.054(9)[a]	0.058	2.466
Si–$I_{4,7}$	2.433(6)	2.450	0.054(9)[a]	0.058	2.466
Si–H	[1.506]	[1.531]	–	0.089	1.482
Torsion independent (anti values)					
$I_3\cdots I_4$	4.027(8)	4.040	0.149(9)[b]	0.152	4.081
$I_7\cdots I_8$	4.027(8)	4.040	0.149(9)[b]	0.152	4.081
$I_3\cdots H_2$	3.269(5)	3.291	–	0.158	3.254
$I_7\cdots H_6$	3.269(5)	3.291	–	0.158	3.254
$I_4\cdots H_2$	3.269(5)	3.291	–	0.158	3.254
$I_8\cdots H_6$	3.269(5)	3.291	–	0.158	3.254
$Si_1\cdots I_7$	3.855(17)	3.866	0.168(10)[b]	0.171	3.896
$Si_5\cdots I_3$	3.855(17)	3.866	0.168(10)[b]	0.171	3.896
$Si_1\cdots I_8$	3.855(17)	3.866	0.168(10)[b]	0.171	3.896
$Si_5\cdots I_4$	3.855(17)	3.866	0.168(10)[b]	0.171	3.896
$Si_5\cdots H_2$	3.217(27)	3.232	–	0.176	3.174
$Si_1\cdots H_6$	3.217(27)	3.232	–	0.176	3.174
Torsion dependent					
Anti conformer					
$H_2\cdots H_6$	4.437(23)	4.456	–	0.177	4.373
$I_7\cdots H_2$	4.143(19)	4.157	–	0.311	4.186
$I_4\cdots H_6$	4.143(19)	4.157	–	0.311	4.186
$I_8\cdots H_2$	4.143(19)	4.157	–	0.311	4.186
$I_3\cdots H_6$	4.143(19)	4.157	–	0.311	4.186
$I_3\cdots I_7$	6.001(13)	6.007	0.167(17)[c]	0.151	6.091
$I_4\cdots I_8$	6.001(13)	6.007	0.167(17)[c]	0.151	6.091
$I_3\cdots I_8$	4.449(20)	4.460	0.319(20)[c]	0.304	4.522
$I_4\cdots I_7$	4.449(20)	4.460	0.319(20)[c]	0.304	4.522
Gauche conformer					
$H_2\cdots H_6$	3.650(28)	3.659	–	0.247	3.600
$I_7\cdots H_2$	4.080(19)	4.089	–	0.288	4.058
$I_4\cdots H_6$	4.080(19)	4.089	–	0.288	4.058
$I_8\cdots H_2$	5.210(15)	5.222	–	0.155	5.225
$I_3\cdots H_6$	5.210(15)	5.222	–	0.155	5.225
$I_3\cdots I_7$	4.476(20)	4.488	0.299(20)[c]	0.283	4.665
$I_4\cdots I_8$	4.476(20)	4.488	0.299(20)[c]	0.283	4.665
$I_3\cdots I_8$	4.575(20)	4.594	0.309(20)[c]	0.294	4.677
$I_4\cdots I_7$	5.968(13)	5.973	0.159(17)[c]	0.144	6.047

[a–c] These vibrational amplitudes were refined in groups.

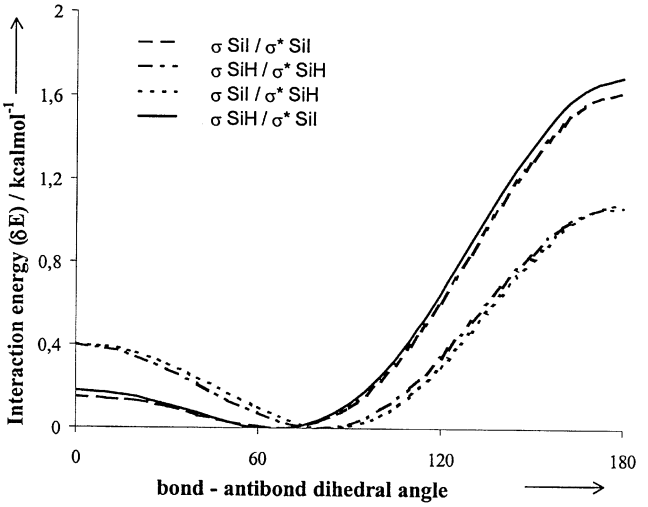

Fig. 10. Calculated bond–antibond interaction energies (δE_σ) of DIDS as a function of the dihedral angle between the bonds σSIIσ*SiI, σSiHσ*SiH, σSIIσ*SiH and σSiHσ*SiI. Note that a higher positive value represents a higher lowering of the potential energy (cf. Eq. (6)).

not the dipole dipole repulsions which determine the conformer stability of DIDS. It is of some note, however, that the ab initio calculations predict dihedral angles >60° for *gauche* DIDS at all levels of theory (HF, MP2, DFT).

Steric interactions between the two iodine atoms of DIDS are expected to stabilize the *gauche* conformation. Published van der Waals radii for iodine range between 1.95–2.12 Å [43], and the smallest intermolecular iodine–iodine distances for hexaiododisilane (solid state) are between 4.26–4.55 Å, giving a van der Waals radius of 2.13–2.27 Å [44]. Obviously, the negative partial charge located on an iodine atom bonded to the electropositive silicon atom increases its effective size to some extent. For *anti* DIDS, the I···I nonbonded distance is 5.984 Å (r_g; see Table 15), whereas for the *gauche* conformer it is 4.555 Å, close to the van der Waals minimum. The steric interactions thus favour *gauche* if it is anticipated that H···H and H···I interactions play a negligible role. For TIDS, the results are very similar. As expected, bond–antibond interaction energies do not differ significantly from those of DIDS, resulting in an intrinsic barrier that shows no preference for either conformer. Dipole dipole repulsions will stabilize *anti*, while steric interactions should favour the *gauche* conformation, because there are three nonbonded I···I distances close to the van der Waals minimum (cf. Table 16), but only two for the *anti* conformer.

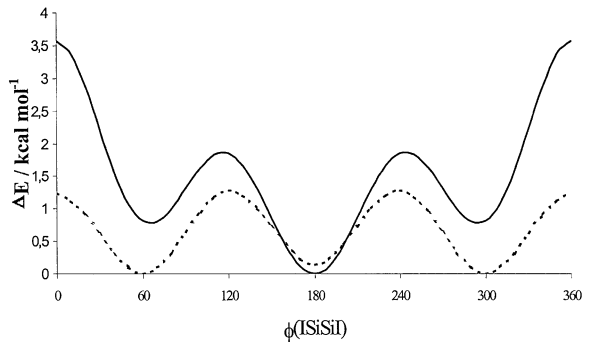

Fig. 11. Calculated potential energy (kcal mol^{-1}) of DIDS as a function of the I–Si–Si–I dihedral angle ϕ (solid line), and approximate intrinsic barrier obtained by summing up all bond antibond interactions.

In Table 13 the conformer compositions for three iododisilanes; the two title compounds along with 1,1,2-triiododisilane [1], have been listed, as obtained from GED refinements, variable-temperature Raman experiments, and the theoretical calculations. The conformational mixtures calculated at the temperatures of experiment seen in Table 13 did not give a convincing or consistent impression, although the data for TIDS agreed slightly better overall than the corresponding data for DIDS. This could be due to an overestimation of the Si–I bond dipole because of the

restricted basis sets available for the iodine atom in conjunction with effective core potentials. For instance, no *triple zeta* basis set is available. The corresponding data on TIDS gave an overall impression that the composition should favour, more or less, the *gauche* conformer, although the actual sign on the ΔE value is very uncertain. However, the observed trend of higher *gauche* stability in progressing from DIDS to TIDS was in accordance with the quantum-mechanical calculations.

A demonstration of the effects on conformational change in increasing the central bond length in ethane type molecules may be seen from data on 1,2-diiodoethane [32] and DIDS. The C–C bond distance (r_g) in 1,2-diiodoethane was found to be 1.479(33) Å from GED data, while the Si–Si bond length in DIDS was 2.315(26) Å (*anti*; present work). In 1,2-diiodoethane, the conformational composition was heavily dominated by the *anti* conformer, with 88(12)% contribution, and a *gauche* torsional angle of 79(16)°. On the other hand, DIDS was found as a mixture consisting of 60% *gauche* conformer, and with a *gauche* torsional angle of 61° obtained from the potential parameters using Eq. (5). The B3LYP torsional angle was about 71° (cf. Table 14). Molecular mechanics (MM) calculations [45] supported the 1,2-diiodoethane GED results, with an estimated 93% of the *anti* conformer for this molecule, and an estimated 80% *gauche* conformer for DIDS. The *gauche* preference in the latter molecule was not reproduced by the ab initio MO and DFT calculations (cf. Table 14). The I···I *gauche* non-bonded distance range found in the refined minimum-energy GED structures of both DIDS and TIDS in the present work was 4.44–4.57 Å. This observed distance range agrees well with the value of 4.45 Å found by Røhmen in the fitting of Morse potential parameters for this particular non-bonded interaction to be used in MM calculations [45].

The use of different force fields, or different modifications of the same force field, will have an impact on the final results. This is because various force fields give slightly different values for the shrinkage corrections used in the GED refinements. It is interesting to compare, for instance, the torsional force constants obtained by MM calculations with the corresponding values obtained from symmetrized ab initio force fields (HF/ 6-31G(d)/HW-ECP(I)). The torsional force constants, F_ϕ, obtained for *anti* and *gauche* DIDS by Røhmen et al. using MM [4] were 0.060 and 0.064 mdyn Å rad^{-2}, respectively. The authors reported calculated torsional frequencies of 36 and 25 cm^{-1} for *anti* and *gauche* DIDS, respectively, based on these values for F_ϕ. In the present work, we have found F_ϕ (*anti*, DIDS) = 0.051 mdyn Å rad^{-2} and F_ϕ (*gauche*, DIDS) = 0.045 mdyn Å rad^{-2}, from the (unscaled) HF/HW-ECP(I) calculations. The NCA gave torsional frequencies of 34 and 26 cm^{-1}, for *anti* and *gauche* DIDS, respectively. These values were indeed very similar to the ones reported by Røhmen et al. [4]. However, for TIDS larger differences between the methods were found, as the F_ϕ values (mdyn Å rad^{-2}) obtained from MM were 0.113 (*anti*) and 0.133 (*gauche*), while the ab initio symmetrized values became 0.087 (*anti*) and 0.080 (*gauche*). These values for the torsional force constants resulted in lower torsional frequencies obtained from the ab initio MO calculations than obtained from the MM calculations. None of the torsional modes for either DIDS or TIDS could be observed experimentally by IR and Raman spectroscopy [5]. The final scaled (refined) ab initio MO force fields gave torsional frequencies almost identical to the original (unscaled) values, indicating that these modes were not heavily mixed with other normal modes of either molecule. The general valence force field used in the previous GED work [4] seemed reasonable overall, compared to the symmetrized diagonal values from the HF/HW-ECP(I) force fields utilized in the present work. However, the utilized valence-field force constant for Si–I stretch was only 1.30 mdyn Å^{-1} [4], which was somewhat low compared to the range found from the present ab initio MO results, which was 1.8–2.0 mdyn Å^{-1}. The calculated shrinkage and vibrational amplitude values obtained by Røhmen et al. [4] agreed quite well with corresponding values obtained in the present work, when all normal modes were included in the NCA. The vibrational amplitudes and perpendicular correction values ($K + \delta r$) for the non-bonded interactions were both significantly lowered by removing the torsional mode. However, the vibrational amplitudes for the bonded distances were practically unchanged by this modification, while the perpendicular corrections were not. The differences were larger for the *gauche* interactions (as opposed to the

anti interactions) of either conformer for both molecules. For instance, in the static DIDS refinements, the vibrational amplitudes became $\mathcal{l}^{\exp}(I\cdots I)_{anti} = 0.177(55)$ Å (calc. 0.130 Å) and $\mathcal{l}^{\exp}(I\cdots I)_{gauche} = 0.430(57)$ Å (calc. 0.383 Å), compared to the lower values $\mathcal{l}^{\exp}(I\cdots I)_{anti} = 0.161(59)$ Å (calc. 0.130 Å) and $\mathcal{l}^{\exp}(I\cdots I)_{gauche} = 0.302(60)$ Å (calc. 0.271 Å) obtained in the dynamic model refinements. At last, we note that while the calculated perpendicular correction value of 0.008 Å for the Si–Si bond distance in TIDS by Røhmen et al. [4] was identical to the present value (*anti*; unaffected by the presence or the absence of the torsional mode, but not unaffected by conformational change), the corresponding value for DIDS was 0.017 Å in the previous work [4], compared to the present value of only 0.004 Å (*anti*; also unaffected by the torsional mode).

It was hoped that the improved models in the present work would remove some of the discrepancies between the earlier reported, and surprisingly larger, Si–Si bond distances [4] and the values obtained for this bond in recent works [1,2], which were more consistent with established experimental data [6–15]. We have in the present work obtained experimental values that falls more into the normal range observed for this type of bond, judging from the set of data found in the literature [6–15]. Our results, with r_g(Si–Si) = 2.315(26) and 2.325(26) Å for *anti* and *gauche* DIDS, respectively, and with r_g(Si–Si) = 2.364(30) and 2.363(30) Å for *anti* and *gauche* TIDS, respectively, compare well to the values found in 1,1,2,2-tetrachlorodisilane [2] and 1,1,2-triiododisilane [1], with the more recent value of 2.363(3) Å found for this bond distance (r_a) in octamethylcyclotetrasilane (Si_4Me_8) [46], and with the value of 2.342(9) Å found in hexamethyldisilane [47]. In the solid-state X-ray study of hexaiododisilane the value 2.323(4) Å was reported [44]. All of these values were found lower than the range of 2.380–2.389 Å reported for the Si–Si bond distance (r_g) in the previous work [4].

The main conclusion regarding obtained experimental energy barrier heights was that both experimental and theoretical methods indicated an increase in the barrier heights in going from the diiodo- to the tetraiododisilane compound. The barriers to internal rotation in 1,1,2-triiododisilane [1] was found quite 'flat', giving a much more even distribution of pseudoconformers than in DIDS and TIDS. Unfortunately, potential energy considerations for iododisilane compounds should be performed with great caution, as large experimental errors greatly limits the reliability of the results presented here.

5. Conclusions

1. The Si–Si distances in the previous work by Røhmen et al. [4] are most probable too large. The Si–Si bond distance in DIDS is in all probability similar to the values observed in 1,1,2-triiododisilane [1] and 1,1,2,2-tetrachlorodisilane [2] (range of 2.310–2.329 Å).
2. The Si–Si distance in TIDS is larger than in DIDS, with a value more similar to the one found in strained or heavier substituted molecules, like octamethylcyclotetrasilane [46], 1,1,2,2-tetrabromodisilane [11] or hexamethyldisilane [47] (range of 2.342–2.363 Å).
3. The trend in conformer stability in the present GED investigation was found in accordance with the calculated trend using DFT and HF methods (with effective core potentials). The trend was in favour of a higher *gauche* stability in progressing from the DIDS to the TIDS molecule. The GED and Raman data agreed on a *gauche* conformer preference for both molecules.

Acknowledgements

We are very grateful to Hans Vidar Volden and Snefrid Gundersen at the University of Oslo for recording the original electron diffraction data in 1991. This work has received support from The Research Council of Norway (Program for Supercomputing) through grants of computing time.

References

[1] T.H. Johansen, K. Hagen, K. Hassler, G. Tekautz, R. Stølevik, J. Mol. Struct. 509 (1999) 237.
[2] T.H. Johansen, K. Hagen, R. Stølevik, J. Mol. Struct. 485-486 (1999) 121.
[3] M. Ernst, K. Schenzel, A. Jähn, W. Köll, K. Hassler, J. Raman Spectrosc. 28 (1997) 589.

[4] E. Røhmen, K. Hagen, R. Stølevik, K. Hassler, M. Pöschl, J. Mol. Struct. 244 (1991) 41.
[5] K. Hassler, M. Pöschl, Spectrochim. Acta 47A (1991) 439.
[6] B. Beagley, A.R. Conrad, J.M. Freeman, J.J. Monaghan, B.G. Norten, G.C. Holywell, J. Mol. Struct. 11 (1972) 371.
[7] A.P. Cox, R.J. Varma, Chem. Phys. 44 (1966) 2619.
[8] J. Pasinski, S.A. McMahon, R. Beaudet, J. Mol. Spectrosc. 55 (1975) 88.
[9] H. Oberhammer, J. Mol. Struct. 31 (1976) 237.
[10] J. Haase, Z. Naturforsch 28A (1973) 542.
[11] H. Thomassen, K. Hagen, R. Stølevik, K. Hassler, J. Mol. Struct. 47 (1986) 331.
[12] J.R. Durig, J.S. Church, Y.S. Li, Inorg. Chem. 21 (1982) 35.
[13] A. Haaland, K. Rypdal, H. Stüger, H.V. Volden, Acta Chem. Scand. 48 (1994) 46.
[14] A. Almenningen, T. Fjeldberg, J. Mol. Struct. 77 (1981) 315.
[15] T.H. Johansen, K. Hagen, R. Stølevik, M. Ernst, K. Hassler, J. Mol. Struct. 372 (1995) 161.
[16] W.R. Wadt, Hay, J. Chem. Phys. 82 (1985) 284.
[17] W. Stephens, H. Basch, Krauss, J. Chem. Phys. 81 (1984) 6026.
[18] W. Stephens, J. Krauss, H. Basch, P.G. Jasien, Can. J. Chem. 70 (1992) 612.
[19] W. Zeil, J. Haase, L. Wegmann, Z. Instrumentenkd. 74 (1966) 84.
[20] L. Hedberg, Abstracts of Papers, Fifth Austin Symposium on Gas-Phase Molecular Structure, Austin, TX, March 1974, p. 37.
[21] A.W. Ross, M. Fink, R. Hilderbrandt, International Tables of Crystallography, vol. 4, Kluwer Academic Publishers, Dordrecht, 1992 p. 245.
[22] M.J. Frisch, G.W. Trucks, H.B. Schlegel, P.M. W. Gill, B.G. Johnson, M.A. Robb, J.R. Cheeseman, T. Keith, G.A. Petersson, J.A. Montgomery, K. Raghavachari, M.A. Al-Laham, V.G. Zakrzewski, J.V. Ortiz, J.B. Foresman, J. Cioslowski, B.B. Stefanov, A. Nanayakkara, M. Challacombe, C.Y. Peng, P.Y. Ayala, W. Chen, M.W. Wong, J.L. Andres, E.S. Replogle, R. Gomperts, R.L. Martin, D.J. Fox, J.S. Binkley, D.J. Defrees, J. Baker, J.P. Stewart, M. Head-Gordon, C. Gonzalez, J.A. Pople, GAUSSIAN 94, Revision D.4, Gaussian Inc., Pittsburgh, PA, 1995.
[23] E.B. Wilson Jr., J.C. Decius, P.C. Cross, Molecular Vibrations, McGraw-Hill, New York, 1955.
[24] L. Hedberg, I.M. Mills, J. Mol. Spectrosc. 160 (1993) 117.
[25] L. Hedberg, I.M. Mills, J. Mol. Spectrosc. 203 (2002) 82.
[26] P. Klaboe, Vibrational Spectrosc. 9 (1995) 3.
[27] K. Hedberg, in: J. Laane, M. Dakkouri, B. van der Veken, H. Oberhammer (Eds.), Structures and Conformations of Non-Rigid Molecules, NATO ASI series C, vol. 410, Kluwer Academic Publishers, Netherlands, 1993, pp. 423–445.
[28] K. Hedberg, M. Iwasaki, Acta Crystallogr. 17 (1964) 529.
[29] L.S. Bartell, J. Chem. Phys. 38 (1963) 1827.
[30] K. Kuchitsu, Y. Morino, Bull. Chem. Soc. Jpn 38 (1965) 841.
[31] K. Kuchitsu, M. Nakata, S. Yamamoto, in: I. Hargittai, M. Hargittai (Eds.), Stereochemical Applications of Gas-Phase Electron Diffraction, VCH Publishers, Incorporate, New York, 1988, pp. 235–236 Part A, Table 7-2.
[32] E. Røhmen, K. Hagen, R. Stølevik, J. Tremmel, J. Mol. Struct. 243 (1991) 419.
[33] J. Dale, Stereochemistry and Conformational Analysis, Universitetsforlaget, Oslo, 1978 pp. 104–105.
[34] T.K. Brunck, F. Weinhold, J. Am. Chem. Soc. 101 (1979) 1700.
[35] A.E. Reed, F. Weinhold, Isr. J. Chem. 13 (1991) 277.
[36] R.S. Mulliken, J. Chem. Phys. 7 (1939) 339.
[37] R.S.J. Mulliken, C.A. Rieke, W.G. Brown, J. Am. Chem. Soc. 63 (1941) 41.
[38] F. Neumann, H. Teramae, J.W. Downing, J. Michl, J. Am. Chem. Soc. 120 (1998) 573.
[39] A.E. Reed, L.A. Curtiss, F. Weinhold, Chem. Rev. 88 (1988) 899.
[40] S. Wolfe, Acc. Chem. Res. 5 (1972) 102.
[41] E. Juaristi, J. Chem. Edu. 56 (1979) 438.
[42] P.R. Rablen, R.W. Hoffmann, D.A. Hrovat, W.T. Borden, J. Chem. Soc., Perkin Trans. 2 (1999) 1719.
[43] J.E. Huheey, E.A. Keiter, R.L. Keiter, Anorganische Chemie-Prinzipien von Struktur und Reaktivität, Walter de Gruyter, Berlin, 1995.
[44] M. Jansen, B. Friede, Acta Crystallogr. C52 (1996) 1333.
[45] E. Røhmen, Cand. Scient. Thesis, University of Trondheim, AVH, 1989.
[46] V.P. Novikov, S.A. Tarasenko, S. Samdal, L.V. Vilkov, Struct. Chem. 11 (2000) 111.
[47] B. Beagley, J.J. Monaghan, T.G. Hewitt, J. Mol. Struct. 8 (1971) 401.